

M.S. ABDUL AZIZ¹, M.S. RUSDI^{1*}, M.S. ZUBIR¹, Z. EMBONG², M. NABIALEK³

THE INFLUENCE OF GOLD WIRE QUANTITY ON THE ENCAPSULATION OF LIGHT-EMITTING DIODES

In the realm of high-power LED applications, several critical concerns emerge, significantly impacting LED operational efficiency and reliability. Among these concerns, wire deformation during the LED encapsulation process poses a substantial threat to LED longevity. This research endeavors to investigate the influence of gold wire quantity on the LED encapsulation procedure. Leveraging ANSYS Fluent, our study employs the Volume of Fluid (VOF) technique along with a user-defined function (UDF) to model the deposition of epoxy materials onto the LED. Moreover, ANSYS Fluent is harnessed for a comprehensive analysis of fluid-structure interaction (FSI) phenomena that occur between the gold wire bonding and the epoxy materials. The FSI modeling allows us to indirectly quantify the stress exerted on the gold wire bonding during the encapsulation process. Our simulations encompass a range of gold wire quantities, spanning from 1 to 5, while a validation experiment is conducted to affirm the structural integrity of epoxy materials as per the simulation setup. Our findings reveal a direct correlation between increased epoxy material density and heightened wire deformation, stress levels, and strain distribution on the wire bonding. For EMC, which has the highest density, the maximum gold wire deformation, Von Mises stress, and strain distribution on the gold wire are 2.6616×10^{-8} mm, 0.00064 MPa, and 8.2019×10^{-9} , respectively. Additionally, the simulations underscore that augmenting the number of gold wires exacerbates stress and strain distribution, assuming consistent epoxy material usage. The present study will contribute to the understanding of the mechanical aspects linked with LED encapsulation and present potential opportunities for improving manufacturing procedures and guiding future experimental attempts in this research domain.

Keywords: Computational method; encapsulation process; LED

1. Introduction

Good quality light-emitting diode (LED) devices must have desirable features such as low power consumption and high efficiency, dependability, and life expectancy [1-3]. Other desirable properties include life expectancy. However, it is quite challenging to obtain an LED with the attributes that are desired because several different aspects could potentially alter the device's operation. A study on the encapsulating procedure that is used in LED packaging was carried out by Alim et al. [4]. They outlined several difficulties associated with LED packaging, including the shape of the encapsulation, the thermal conductivity of the packaging material, the deterioration of the packaging material, and the strength of the bonding. Therefore, the failure rates of the LED device can frequently be ascribed to the reasons that will be discussed further below.

The materials that are used for packaging are one of the aspects in which a wide variety of errors could arise. For instance, heat generated by the PN junction of the chip, when mixed with the ambient temperature of the surrounding environment, might cause the material used in the LED's packaging to fracture and change color [5]. Epoxy resins, which are considered to be among the best thermosetting polymer materials, have found widespread application in the modern LED encapsulation process due to the many benefits that they offer, including high adhesive strength, superior machinability, and excellent resistance to chemicals. Shan and Chen's formula [6]. As a result, this article will focus on researching three distinct varieties of epoxy resins that are utilized in the process of encapsulating LEDs.

Epoxy Molding Compound (EMC) is extensively utilized in the electronics sector as a packaging material for encapsulating semiconductor substances. The residual stress will be generated

¹ UNIVERSITI SAINS MALAYSIA, SCHOOL OF MECHANICAL ENGINEERING, ENGINEERING CAMPUS, 14300, NIBONG TEBAL, PENANG, MALAYSIA.

² UNIVERSITI TUN HUSSEIN ONN MALAYSIA (UTHM), FACULTY OF APPLIED SCIENCE AND TECHNOLOGY (FAST), DEPARTMENT OF PHYSICS AND CHEMISTRY, 84600 PANCHOR, MUAR, JOHOR, MALAYSIA

³ CZĘSTOCHOWA UNIVERSITY OF TECHNOLOGY, DEPARTMENT OF PHYSICS, AL. A. KRAJOWEJ 19, 42-200 CZĘSTOCHOWA, POLAND

* Corresponding author: syakirin@usm.my



during the curing process of this material as a result of both cure and thermal shrinkage. This can potentially cause the product to fail [7]. Sadeghinia et al. [7] conducted a study to examine the alterations in both the elastic modulus and viscoelastic properties throughout the curing process. The experimental shear setup involved the utilization of a Dynamic Mechanical Analyzer (DMAQ800) instrument to quantify the alterations in the mechanical characteristics of the EMC.

Wire sweep is a potential failure mode that can happen during wire bonding. Typically, it arises in the context of the transfer molding procedure. Wire sweep, also known as wire deformation, is a significant concern in the transfer molding process. Excessive wire sweep can lead to electrical short circuits and device failure, as the wires come into contact with neighboring wires. Ali et al. [8] conducted a study to examine the properties of wire sweep by analyzing different wire parameters, including wire locations, mold flow directions, wire lengths, wire pitches, and wire angles. The study was performed on Low Quad Flat Packages (LQFP) utilizing the JMP statistical analysis software. According to the results, wire length has the greatest impact on wire sweep percentage compared to the other parameters. According to this study, it has been determined that using a shorter wire length is a more appropriate option for wire bonding compared to using a longer wire. The increase in wire length during wire bonding leads to a higher percentage of wire sweep during the transfer molding process.

Failures can occur at the wire bonding for a variety of reasons, including wire deformation or wire sweep, for example. When an excessive amount of tension is applied to the wire bonding, it will cause the wire to break, which will ultimately result in the LED gadget being rendered inoperable [9]. During the process of encapsulation, the creation of wire sweeps can be caused by several different circumstances. As a result, one of the primary focuses of this article will be an investigation of how the amount of gold wires affects LED. On the market right now, you may choose from a few different kinds of encapsulation structures for LED lights. The kind of LED that is being encased determines the particular kind of encapsulation structure that will be utilized during the process [10]. In the course of this research, a standard LED encapsulation structure, which takes the form of a half-sphere will be utilized.

The present study introduces an innovative methodology for investigating the encapsulation process of light-emitting diodes (LEDs) through the utilization of computer modeling techniques. This study employs a hybrid methodology that combines computational analysis with experimental validation to examine the effects of varying numbers of gold wires on the process of LED encapsulation. The main aim of this study is to validate the results acquired using these methodologies. During the simulation phase, a comprehensive examination of the LED encapsulation process is conducted, with a specific emphasis on a representative fluid-structure interaction (FSI) model. The intricate problem of encapsulating LEDs within a protective plastic case is resolved by utilizing ANSYS Fluent to permit a comprehensive investigation of the interplay between fluid dynamics

and structural deformation. The findings not only contribute to our comprehension of the mechanical aspects associated with LED encapsulation but also present potential opportunities for enhancing manufacturing procedures and directing forthcoming experimental endeavors in this domain.

2. Methodology

2.1. Governing equation

The Volume of Fluid (VOF) method in simulation software (ANSYS Fluent) was used to simulate the encapsulation process of the LED during the virtual modeling process. This method was used to simulate the process. The VOF method is utilized to perform an analysis on the epoxy resin that is dispensed onto the LED as well as the interaction that takes place during the process between various epoxy resins and gold wire. During the simulation, the fluid flow movement of the epoxy resins can be described with the help of three-dimensional incompressible flow transport equations. These equations include continuity (conservation of mass), Navier-Stokes, Newtonian fluids, and conservation of energy equations. The equations are presented in the following form:

Continuity (conservation of mass) equation [12-14]:

$$\frac{\partial u}{\partial x} + \frac{\partial v}{\partial y} + \frac{\partial w}{\partial z} = 0 \quad (1)$$

where u , v , and w are velocities of the fluid that flow in the x , y , and z axis respectively.

The Navier-Stokes equation for x -direction:

$$\begin{aligned} \frac{\partial u}{\partial t} + u \frac{\partial u}{\partial x} + v \frac{\partial u}{\partial y} + w \frac{\partial u}{\partial z} = -\frac{1}{\rho} \frac{\partial P}{\partial x} + \\ + \left[\frac{\partial}{\partial x} \left(\eta \frac{\partial u}{\partial x} \right) + \frac{\partial}{\partial y} \left(\eta \frac{\partial u}{\partial y} \right) + \frac{\partial}{\partial z} \left(\eta \frac{\partial u}{\partial z} \right) \right] + g_x \end{aligned} \quad (2)$$

The Navier-Stokes equation for y -direction:

$$\begin{aligned} \frac{\partial v}{\partial t} + u \frac{\partial v}{\partial x} + v \frac{\partial v}{\partial y} + w \frac{\partial v}{\partial z} = -\frac{1}{\rho} \frac{\partial P}{\partial y} + \\ + \left[\frac{\partial}{\partial x} \left(\eta \frac{\partial v}{\partial x} \right) + \frac{\partial}{\partial y} \left(\eta \frac{\partial v}{\partial y} \right) + \frac{\partial}{\partial z} \left(\eta \frac{\partial v}{\partial z} \right) \right] + g_y \end{aligned} \quad (3)$$

The Navier-Stokes equation for z -direction:

$$\begin{aligned} \frac{\partial w}{\partial t} + u \frac{\partial w}{\partial x} + v \frac{\partial w}{\partial y} + w \frac{\partial w}{\partial z} = -\frac{1}{\rho} \frac{\partial P}{\partial z} + \\ + \left[\frac{\partial}{\partial x} \left(\eta \frac{\partial w}{\partial x} \right) + \frac{\partial}{\partial y} \left(\eta \frac{\partial w}{\partial y} \right) + \frac{\partial}{\partial z} \left(\eta \frac{\partial w}{\partial z} \right) \right] + g_z \end{aligned} \quad (4)$$

where

- ρ – density,
- u – velocity vector in x -direction,
- v – velocity vector in y -direction,
- w – velocity vector in z -direction,

P – static pressure,
 t – time,
 η – viscosity,
 g_x, g_y and g_w – gravity in x, y and z -axis.

The epoxy viscosity is assumed to be constant at high temperatures. So, the Newtonian fluid equation [15,16]:

$$\eta = \frac{\tau}{\gamma} \quad (5)$$

where

τ – shear stress

γ – strain rate

In order to accurately determine and explain the distribution of the liquid phase, the VOF model makes use of a scalar F in each cell of the computational network [17]. The proportion of the cell's volume that is filled with epoxy material is represented in model by the variable F . This variable can be thought of as a fraction. Therefore, F will have a value of 1 in the cells that contain only the resin, a value of 0 in the cells that are devoid of resin, and a value that is somewhere in the middle of 0 and 1 will be found in the cells that are considered to be "interface" cells and are known as the epoxy flow front. As time goes on, the transport equation will represent the epoxy flow front in its entirety [16]:

$$\frac{dF}{dt} = \frac{\partial F}{\partial t} + u \frac{\partial F}{\partial x} + v \frac{\partial F}{\partial y} + w \frac{\partial F}{\partial z} - \left\{ \frac{\partial^2 F}{\partial x^2} + \frac{\partial^2 F}{\partial y^2} + \frac{\partial^2 F}{\partial z^2} \right\} = 0 \quad (6)$$

One of the methods that can be used to manage the analysis and simulation of the interaction between a fluid (such as epoxy resin) and a solid body (such as gold wire) is called FSI modeling. This is because the stress and strain that is put on gold wire structures during experimental tests are difficult to assess. This is especially true for LED applications. As a consequence of this, the methodology entails a very good method for observing how the epoxy resin and the gold wire bonding structures interact with one another. During the process of encapsulant dispensing, the gold wire structures could potentially undergo deformation and wire sweep as a consequence of the stress and strain that is applied to them when an epoxy fluid comes into contact with a solid body. To simulate both the fluid flow and the deformation of a solid structure, you will need both the Navier-Stokes equation and the solid mechanics equation for the deformation of the solid structure. This is because both of these equations describe the deformation of solid structures.

2.2. Computational Setup

The configuration illustrated in Fig. 1 is considered crucial because of its comprehensive methodology in simulating a high-power LED package. The selection of this configuration is based on its ability to accurately represent geometry, which is

accomplished using SolidWorks software. The accuracy of the LED package's dimensions is crucially dependent on precision. The reason for this is that it is necessary to compare our computational data with experiments or high-fidelity computational methods, whenever feasible, to evaluate the error or uncertainty in our predictions[18]. Once the geometry is created in SolidWorks, it can be exported to ANSYS Workbench for simulation execution. The "Boolean" function in Design Modeler is used to exclude components such as the chip, simplifying the setup of the simulation. Significantly, in this context, fluidic elements such as the domain and dispensing needle are categorized as components of the fluid body, whereas solid components like gold wires are classified as part of the solid body. This differentiation is crucial for maintaining accuracy in the simulation. This systematic configuration enhances precision, which is essential for dependable simulation results.

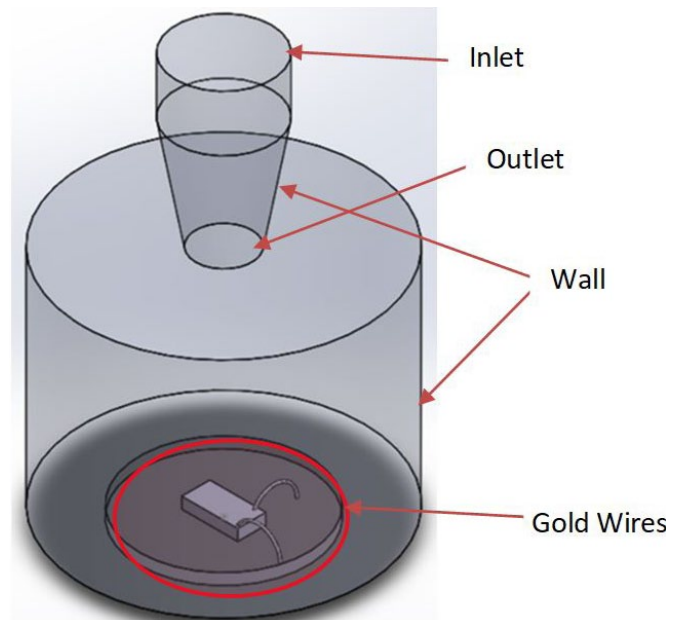


Fig. 1. LED Geometry in SolidWorks

In order to do the calculation of the numerical model for each node that has been produced, the 3D domain that has been created first needs to be divided into a computational mesh, as illustrated in Figs. 2 and 3. Because of the intricate nature of the design, the fluid body was modeled in Fluent using the tetrahedral approach and the linear element order to cut down on the amount of time required for the computation. In the transient structure, the method for the mesh that is utilized is the hexahedral cell with linear element order. This method is employed for the solid body. The statistics of the meshing that were obtained for the fluid body are as follows: 19560 nodes and 98174 elements, whereas the statistics for the meshing that were acquired for the solid body (gold wire number = 2) are as follows: 36513 nodes and 41760 elements. The smoothing quality of every mesh has been increased to a high setting.

It has been determined that the effect that the turbulent flow has on the process of encapsulation dispensing can be ignored in

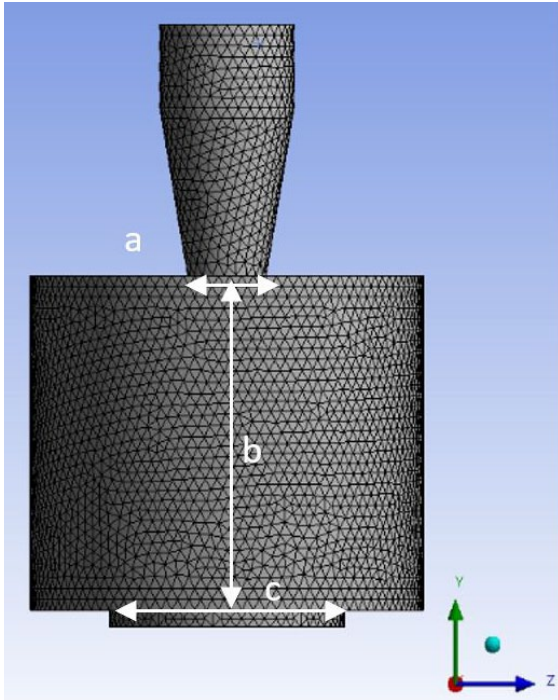


Fig. 2. Tetrahedral Free Mesh Method with Element Size = 0.15 mm

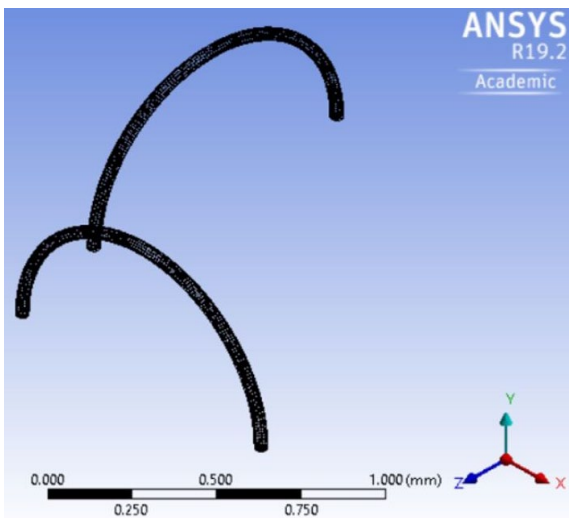


Fig. 3. Hexahedral Free Mesh Method with Element Size = 0.06 mm

the simulation setting [10]. 1.57, 1.21, and 0.39 are the respective values that represent the Reynolds number for the ERL-4221, EMC, and D.E.R.-331. As a result, we are going to assume that the flow is laminar. This is because there are no obstructions or sharp corners that could cause turbulences, which contribute to the process having a high level of consistency. The Volume of Fluid (VOF) scheme and a transient-based formulation are applied throughout each time step that represents a fraction of the volume. The flow equations are going to be summed up in the volume of a single equation set directly when using the VOF approach, and the interface is going to be tracked using a phase indicator function. When a control volume is filled, an indicator is read to determine whether the interface between two phases, which in this example are air and epoxy resin, has

a value of one or zero. This indication is used to track the interface between the two phases. In the configuration, air is given the value 0 and phase 1 of the setup, while epoxy resin is given the value 1 and phase 2 of the setup. Fig. 4 demonstrates that the region that was patched during Phase 2 is represented by the red section, whereas the region that was patched during Phase 1 is represented by the blue section.

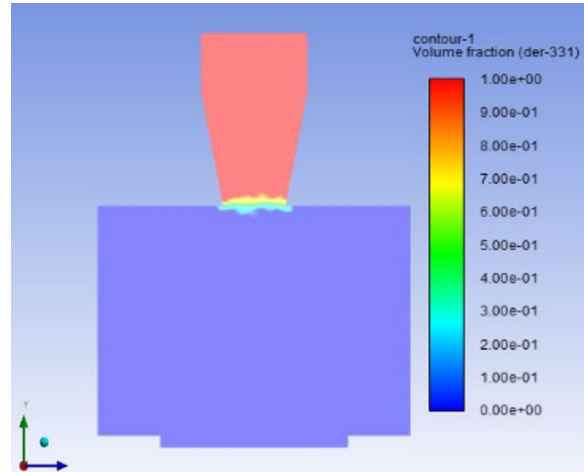


Fig. 4. Patched Volume Fraction of Epoxy Resin

2.3. Grid Independent Test

In order for a computational fluid dynamics (CFD) solver to produce an accurate solution, the mesh must be of sufficient quality and have the appropriate amount of nodes and elements [19]. In order to determine which mesh element size should be used for the simulation analysis, five models with varying element sizes are investigated: Mesh-1 (0.10 mm), Mesh-2 (0.15 mm), Mesh-3 (0.20 mm), Mesh-4 (0.25 mm), and Mesh-5 (0.30 mm). The goal of this investigation is to find the optimal mesh element size. The Von Mises stress that is imparted to two gold wires by EMC is the variable that is used to perform the grid-independent test for the various mesh sizes, as shown in Fig. 5. The statistics on the number of mesh elements and the amount of computational time spent on each model that was utilized in the grid-independent test are presented in TABLE 1.

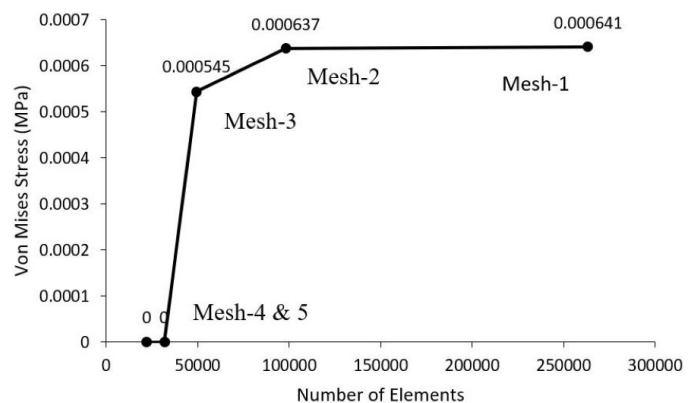


Fig. 5. Von Mises Stress against Number of Elements

TABLE 1
Statistic of Mesh Elements and Computational Time

Mesh Type	Nodes	Elements	Computational Time (hours)
Mesh-1 (0.10 mm)	50998	263380	10
Mesh-2 (0.15 mm)	19560	98174	6
Mesh-3 (0.20 mm)	10082	49418	3
Mesh-4 (0.25mm)	6503	31613	0
Mesh-5 (0.30 mm)	4605	22171	0

The comparison among different mesh types primarily hinges on the maximum von Mises stress value, as delineated in Fig. 5. However, Mesh-4 and Mesh-5 register erroneous stress values of 0 MPa due to the utilization of coarse and suboptimal mesh configurations, evident in Fig. 6. The root cause of this mesh issue lies in the oversized element dimensions, which are incompatible with the model. Consequently, Mesh-4 and Mesh-5 become untenable options.

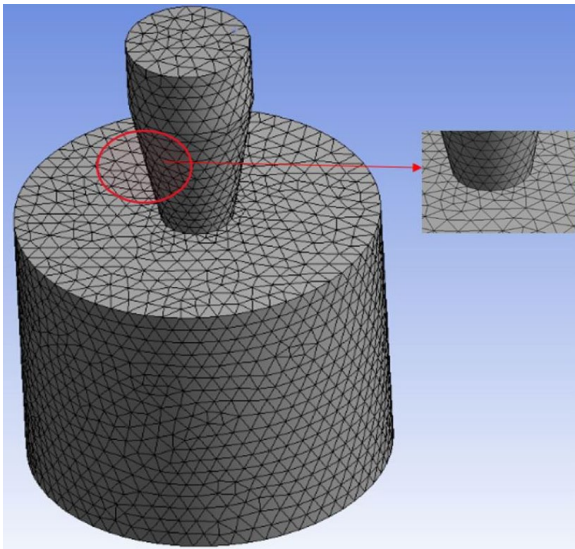


Fig. 6. Mesh Error in Mesh-4 and Mesh-5

Mesh-1, comprising 50,998 nodes and 263,380 elements, demonstrates the highest von Mises stress value of 0.000641 MPa. Conversely, Mesh-2, with 19,560 nodes and 98,174 elements, exhibits a slightly lower maximum von Mises stress of 0.000637 MPa. The disparity between Mesh-1 and Mesh-2 is a mere 0.06%, falling well below the 1% threshold. Mesh-3, featuring 10,082 nodes and 49,418 elements, records the highest von Mises stress value of 0.000545 MPa, with a noticeable difference of 14.44% compared to Mesh-2.

The selection of an appropriate mesh type and size for simulation is influenced by considerations such as computational complexity, convergence, accuracy prerequisites, and time constraints, especially when operating with a step size of $1e-5$. After conducting a grid-independent test, Mesh-2 with 0.15 mm element size was chosen as the benchmark for this study. This choice is rooted in its capability to yield comparable results with negligible percentage error (less than 1%), diverging

significantly from Mesh-3, which exhibits a substantial percentage error of 14.44%.

Furthermore, the computational demands increase in proportion to the cell count employed. Mesh-2's computational time, amounting to 7 hours is notably more efficient than Mesh-1, which consumes 10 hours. In summary, Mesh-2 emerges as the optimal choice due to its energy and time-saving attributes, with an established element size of 0.15 mm

2.4. Material Properties and Boundary Conditions

TABLE 2
Material Properties of EMC [10]

Properties	Epoxy Molding Compound
Density (kg/m^3)	1800
Viscosity (kg/m.s)	0.448
Surface Tension (N/m)	0.005

TABLE 3
Material Properties of D.E.R.-331[20]

Properties	D.E.R.-331
Density (kg/m^3)	1159
Viscosity (kg/m.s)	0.896
Surface Tension (N/m)	0.005

Source: [21]

TABLE 4
Material Properties of ERL-4221[20]

Properties	ERL-4221
Density (kg/m^3)	1173
Viscosity (kg/m.s)	0.224
Surface Tension (N/m)	0.005

TABLE 5
Material Properties of Gold Wire

Properties	Gold Wire
Density (kg/m^3)	19300
Young's Modulus (Pa)	7.85×10^{10}
Poisson's Ratio	0.42
Tensile Yield Strength (Pa)	1.84×10^8
Tensile Ultimate Strength (Pa)	1.99×10^8
Number of Gold Wire	1,2,3,4,5

TABLE 6
Boundary Condition

Boundary Condition	Details
Inlet Speed (m/s)	0.30
Injection Time (s)	0.25
Inlet Contact Angle (degree)	175
Needle Diameter, a (mm)	1.00
Distance Needle to Base, b (mm)	4.00
Base Diameter, c (mm)	3.00

2.5. Experimental Setup

The experiment involving LED encapsulation intends to compare the results that were produced from the simulation with the actual outcomes. The apparatus and materials required for the experiment are as follows: a syringe, a needle with a tip that has a diameter of 1 mm, a high-power LED, fluid, and a vacuum chamber. The experimental setup is depicted in Fig. 7, which may be found here. In order to record the data, a digital camera is placed in front of the needle, in addition to an LED. To begin, the LED package is positioned on a level surface inside the vacuum chamber so that the results will not be influenced by any factors that are external to the experiment. After that, the surface of the LED receives an injection from a syringe with a certain amount of EMCA. The liquid can take the shape of a hemisphere thanks to the mold cavity in the LED substrate. After seeing and recording the fluid dispensing process, the data from the simulation is compared with the observations and recordings made during the procedure.

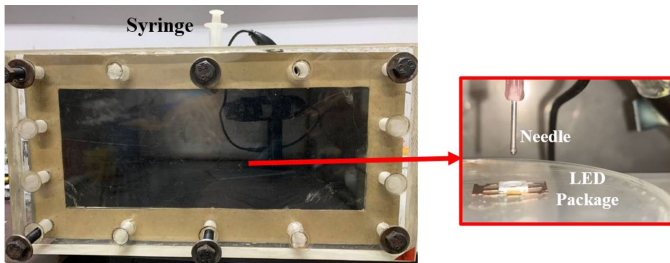


Fig. 7. Experimental setup for LED Encapsulation Process

3. Results and discussion

3.1. Simulation Vs experimental

As both of these fluids have the same viscosity, this section will compare the findings of the simulation of the encapsulant structure using EMC to the results of the experiments using EMC A. Both fluids have the same viscosity. The results of the simulation for the EMC are displayed in Fig. 8, and a comparison of the two structures can be found in TABLE 7.

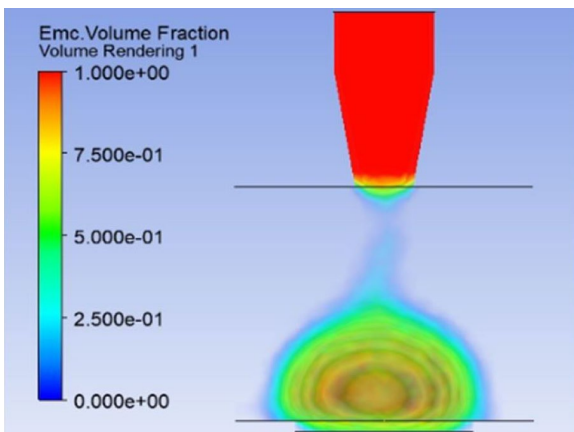


Fig. 8. EMC Simulation Results

3.2. Fluid-Structure Interaction

3.2.1. Effect of Epoxy Materials on Structure of 2 Gold Wires

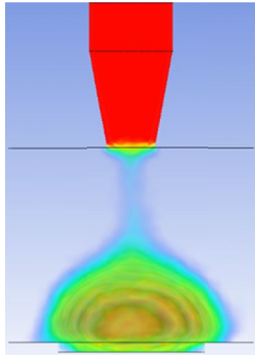
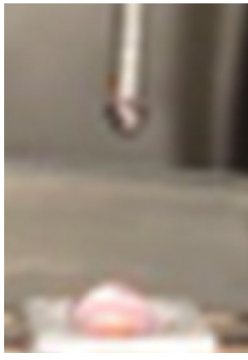
In this part of the article, an investigation into the structural effects of several epoxy resins on two gold wires is carried out. There are three parameters that have been observed, and these are the maximum deformation, the Von Mises stress, and the strain

TABLE 7

Comparison between Simulation and Experimental

Time (%)	EMC	EMCA
0		
10		
25		
60		

TABLE 7. Continued

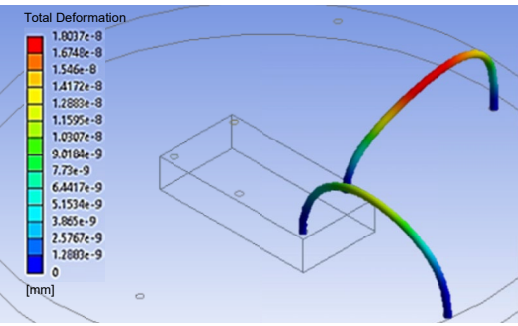
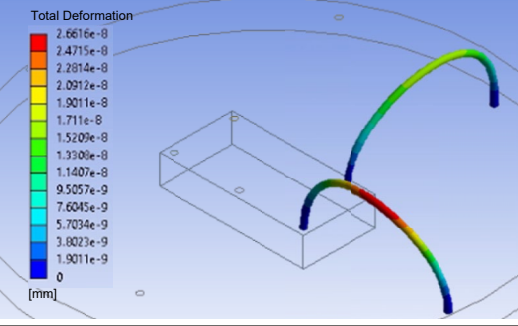
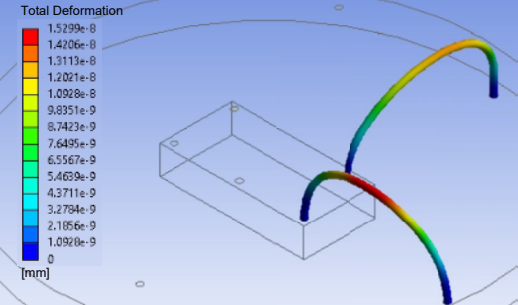
100		
Volume of Epoxy Resin (m ³)	8.51143×10^{-8}	8.97972×10^{-8}
Percentage Difference	5%	

distributions. The findings from the simulation are presented in TABLES 8, 9, and 10.

When the gold wire comes into touch with the epoxy resins that are being dispensed during the encapsulation process, the

TABLE 8

Total Deformation of 2 Gold Wires

Epoxy Resins	Total Deformation (mm)
ERL-4221	
EMC	
D.E.R.-331	

force that results from the pressure of the epoxy resins will induce a certain degree of stress onto the gold wire. The fluid-structure interaction (FSI) approach is used so that the overall deformation, stress, and strain distribution of the gold wires that have been influenced by the force from the epoxy resins can be analyzed. In

TABLE 9

Stress Distributions of 2 Gold Wires

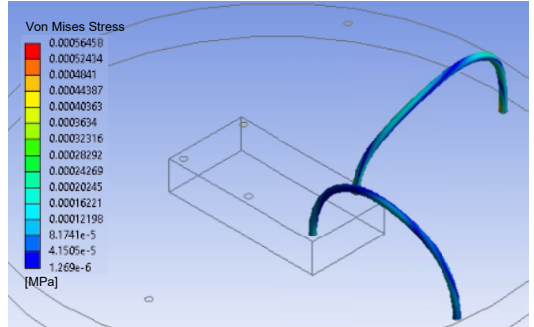
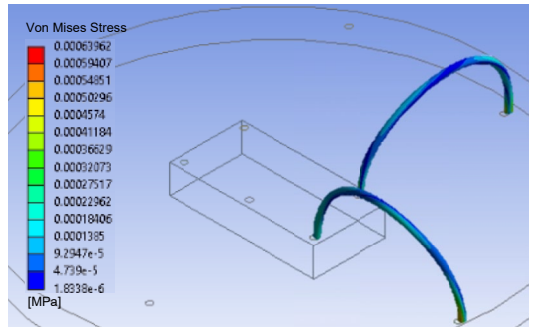
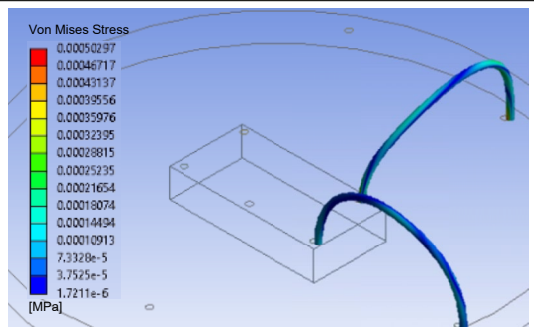
Epoxy Resins	Von Mises Stress (MPa)
ERL-4221	
EMC	
D.E.R.-331	

TABLE 10

Strain Distributions of 2 Gold Wires

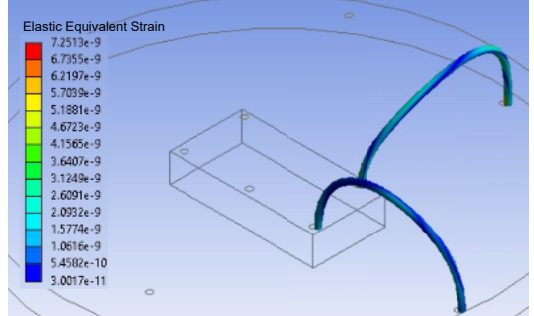
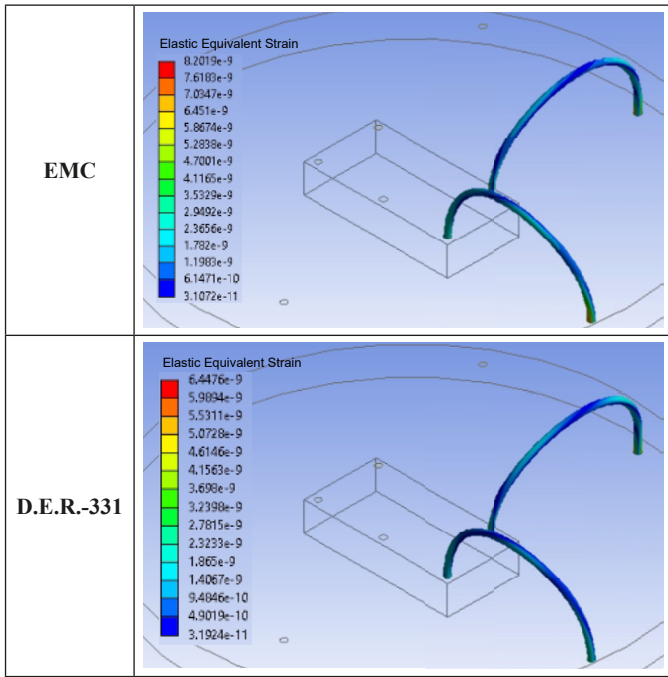
Epoxy Resins	Elastic Equivalent Strain
ERL-4221	

TABLE 9. Continued



TABLES 8, 9, and 10, the results of simulations provide a comparison of the total deformation, stress, and strain distribution for two gold wires using three different types of epoxy resin: ERL-4221, EMC, and D.E.R.-331. These results are based on the results of simulations presented in TABLES 8, 9, and 10.

According to the findings of this particular case study, the values of maximum wire deformation, von Mises stress, and elastic equivalent stress were the highest for D.E.R.-331, but the values for EMC were the highest for maximum wire deformation, von Mises stress, and elastic equivalent stress. Based on the data presented in Fig. 9, the maximum gold wire deformation for ERL-4221, EMC, and D.E.R.-331 was 1.8037×10^{-8} mm, 2.6616×10^{-8} mm, and 1.5299×10^{-8} mm, respectively. In addition, the maximum stress that was induced on the structure of the gold wire by ERL-4221, EMC, and D.E.R.-331 were 0.00056 MPa, 0.00064 MPa, and 0.00050 MPa respectively, while the maximum strain of the gold wire for the three epoxy resins was 7.2513×10^{-9} , 8.2019×10^{-9} and 6.4476×10^{-9} respectively. Figs. 10

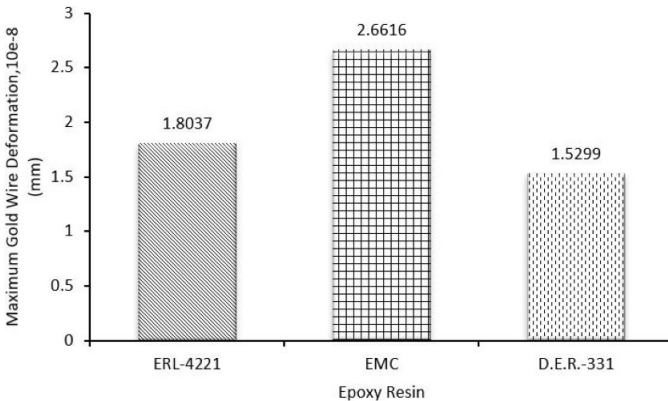


Fig. 9. Maximum Gold Wire Deformation against Three Types of Epoxy Resin

and 11 present a bar chart illustrating the maximum stress and strain spread over the structure of the gold wire for each of the three distinct epoxy resins.

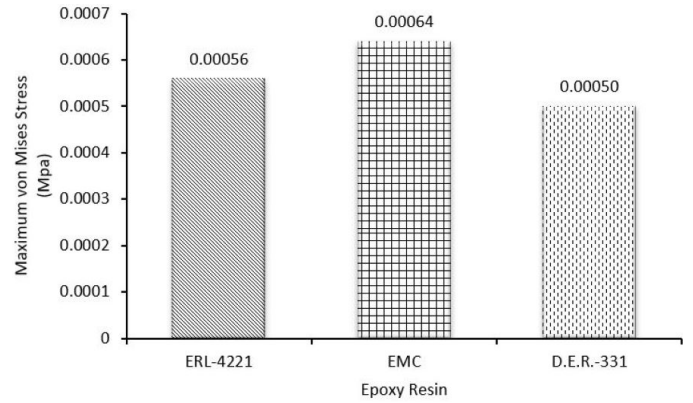


Fig. 10. Maximum von Mises Stress against Three Types of Epoxy Resin

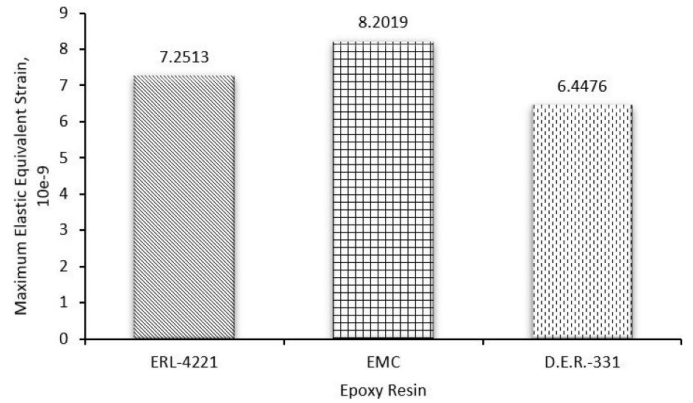


Fig. 11. Maximum Elastic Equivalent Strain against Three Types of Epoxy Resin

According to the findings of an earlier investigation that Ramdan et. al. [9] carried out, they discovered that the effect of the viscosity of the EMC on pressure affected the stresses that were created on the wire structure during the process of encapsulation. Wires that were in touch with EMC that had a high viscosity were subjected to high-pressure distribution, and it was anticipated that they would deform more than wires that had been in contact with EMC that had a low viscosity. Nevertheless, the findings of this case study run counter to the findings of the earlier research because D.E.R.-331, the epoxy with the highest viscosity, had the lowest wire deformation value. This is because the various epoxy resins each possess their own unique set of characteristics. Although the earlier research investigated EMC with varying degrees of viscosity, the density of all EMC remained the same throughout all of the investigations. On the other hand, the epoxy materials that were utilized in this particular research project all had distinct characteristics, with EMC having the highest density and D.E.R.-331 having the lowest density.

According to the results of this investigation, epoxy materials with a higher density, such as EMC, will generate more wire deformation when compared to ERL-4221 and D.E.R.-331.

TABLE 11

Total Deformation of Five Different Gold Wire Numbers by EMC

In most cases, the diameter of the gold wire that was utilized in the process of encapsulating LEDs was somewhere in the range of 18 to 50 micrometers. The tensile strength of this gold wire ranges from 3.0 to 4.7 MPa; however, because of the high purity of the material, the tensile strength can occasionally exceed 7 MPa [22]. In prior work, Chen et al. [23] demonstrated that the bonding of the gold wire can endure maximum stresses of 140.2 MPa at 125°C and 191.4 MPa when the temperature is -40°C. Therefore, the maximum Von Mises Stress that is exerted on the gold wire by the three different epoxy materials is not more than the tensile strength of the gold wire because it is relatively low. Therefore, there have not been any noticeable alterations to the gold wire, and the Von Mises stress that was imposed on the LED by the epoxy resins did not play a significant role in the failure of the LED.

3.2.2. Effect of EMC on Different Gold Wire Number

In this section, the effect of epoxy material, EMC on different gold wire numbers is studied. The same parameters are observed which are maximum deformation, Von Mises stress, and strain distribution TABLE 11, TABLE 12, and TABLE 13.

For this simulation, gold wires with one of the following five different numbers were utilized: 1, 2, 3, 4, and 5. EMC epoxy resin was chosen to be employed for this particular simulation. During the process of encapsulating LEDs, the data generated from the simulations were analyzed, and values of maximum wire deformation, stress, and strain distributions of the gold wire were compared between the various numbers of gold wires. The purpose of this simulation was to investigate the force that was produced as a consequence of the dispensing of the EMC, which results in a certain degree of wire deformation as well as distinct stress and strain values on the structure of the five distinct gold wire numbers. When going from one to three gold wires, there is a proportional rise in both the maximum Von Mises stress and the elastic equivalent strain. However, the value of maximum Von Mises stress and elastic equivalent strain for the gold wires numbered 4 and 5 appears to maintain the same value as the same for the gold wires numbered 3.

The highest stress for each of the five different gold wire numbers was 0.00058 MPa, 0.00064 MPa, 0.00070 MPa, and 0.00070 MPa respectively, whilst the maximum strain for each of the five different gold wire numbers was 7.4546×10^{-9} , 8.2019×10^{-9} , 8.9758×10^{-9} , 8.9758×10^{-9} and 8.9758×10^{-9} . The bar chart for maximum stress and strain distributed on the structure of the gold wire is shown in Figs. 12 and 13. These figures cover a range of five distinct gold wire numbers. LEDs with a higher number of gold wires will experience the highest value for stress and strain during the encapsulation process, as shown by these results. This is in contrast to LEDs with a lesser number of gold wires, which will experience a lower value. When the identical kind of epoxy resin is utilized, the gold wires with a higher number have a greater propensity to distort and fracture at a quicker rate.

Gold Wire Number	Total Deformation (mm)
1	
2	
3	
4	
5	

TABLE 12

Stress Distribution of Five Different Gold Wire Numbers by EMC

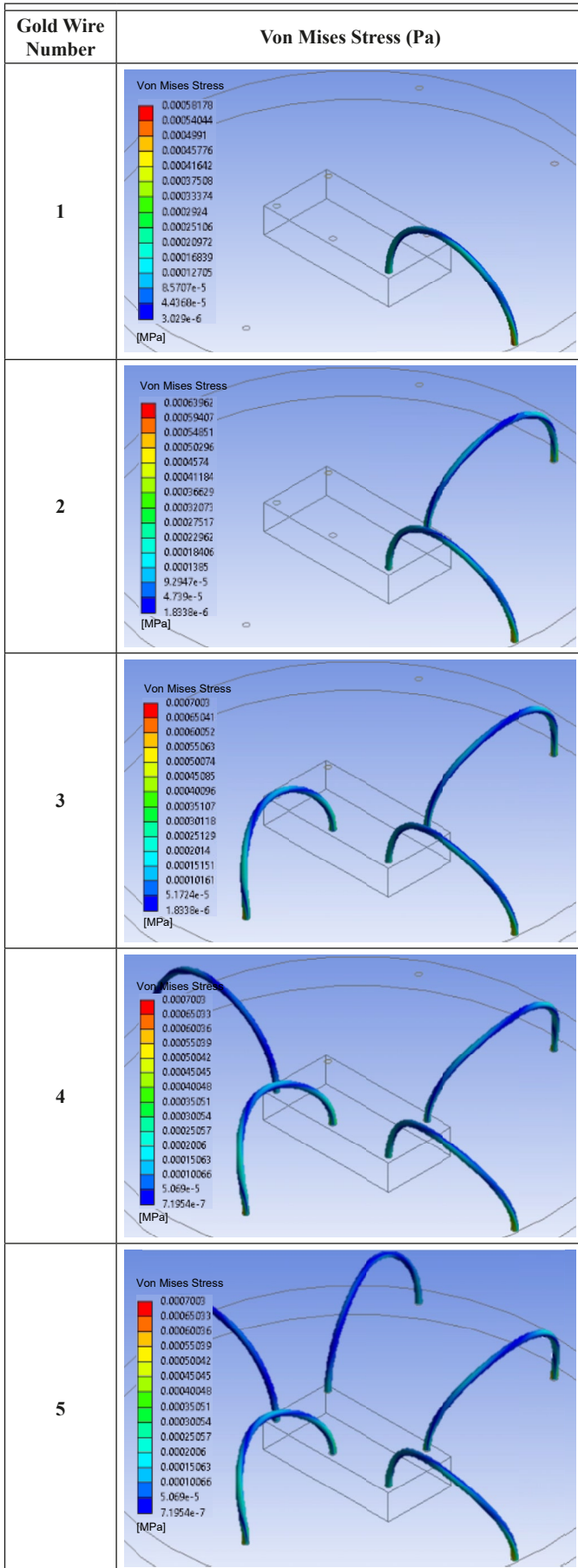
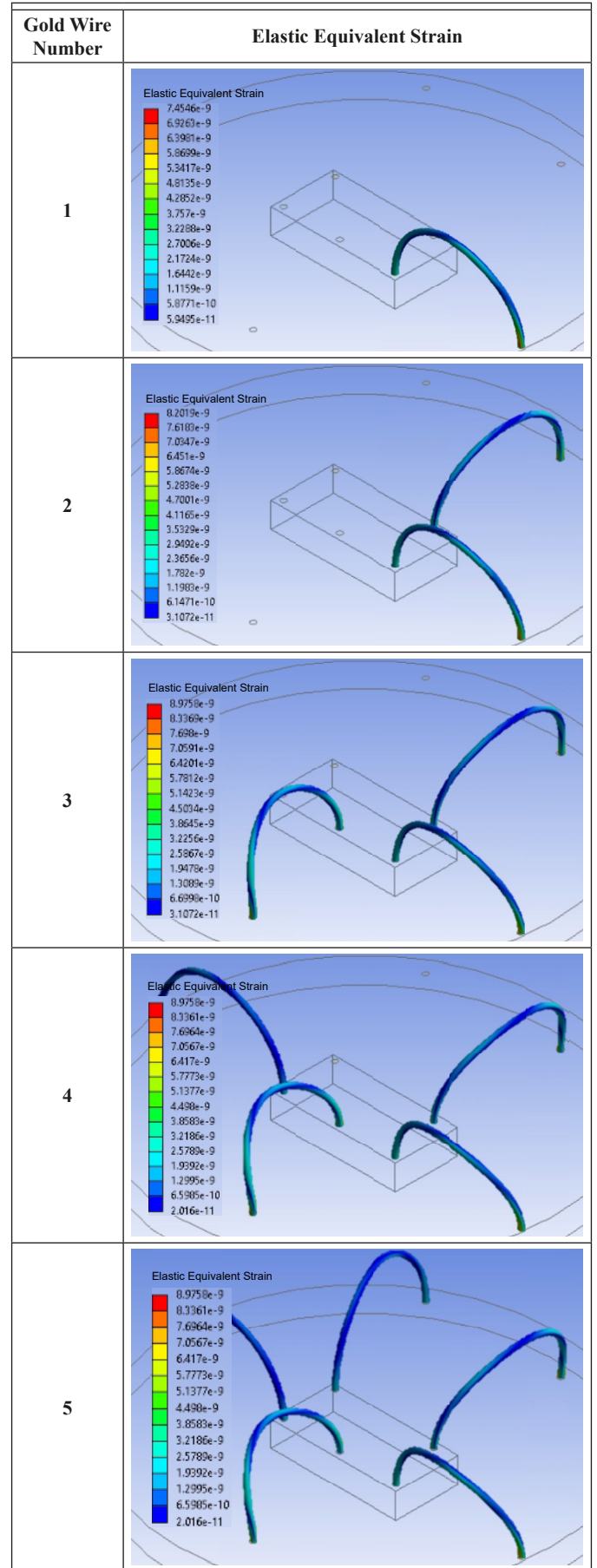


TABLE 13

Strain Distribution of Five Different Gold Wire Numbers by EMC



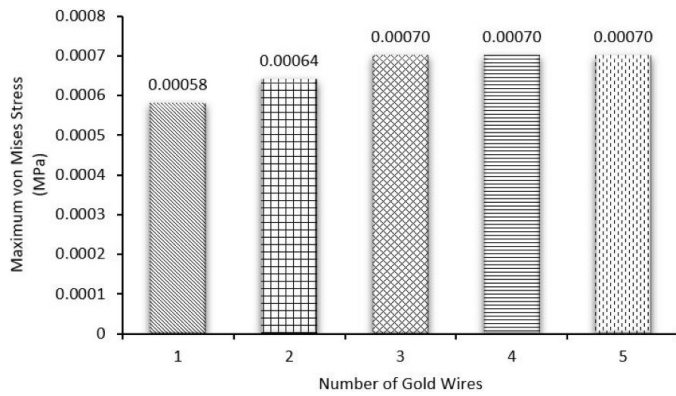


Fig. 12. Maximum von Mises Stress against Number of Gold Wires

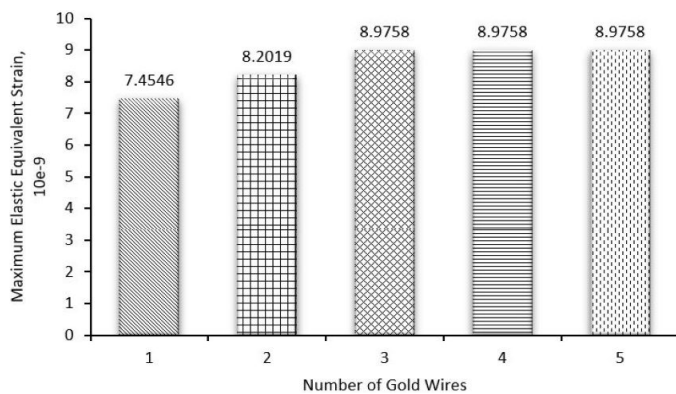


Fig. 13. Maximum Elastic Equivalent Strain against Number of Gold Wires

Due to the very modest levels of maximum stress that the gold wire was subjected to, none of the five cases of the gold wire numbers that were investigated for this study demonstrated any significant modifications. Because the maximum stress measured in any of the cases did not go beyond the yield strength of the gold wire, this finding suggests that the stress did not play a significant role in the failure of the LED.

3.2.3. Future Directions and Limitations

In the future, this study could focus on investigating different encapsulant materials with varying mechanical properties to evaluate how they affect the performance of LED packages. This may involve examining materials that are specifically designed to reduce stress concentrations on internal components, such as gold wire bonding. In addition, more intricate fluid-structure interaction (FSI) simulations could be performed to integrate additional variables such as thermal effects or nonlinear material behaviors, resulting in a more comprehensive comprehension of LED encapsulation dynamics under different operating conditions. In addition, future research could utilize the knowledge acquired from this study to concentrate on enhancing the reliability and performance of LED package designs by taking into account factors such as wire bonding configurations and encapsulant geometry, in addition to epoxy density.

Nevertheless, it is crucial to recognize particular limitations linked to the research. These assumptions, such as linear material behavior and simplified geometries, made during modeling can affect the accuracy and applicability of the findings to more complex LED package designs or materials. Furthermore, the precision of the FSI model and its simulation outcomes relies on the accuracy of the assumptions and boundary conditions employed, which in turn introduces inherent uncertainties or limitations associated with the numerical methodology. Moreover, the study mainly concentrated on the density of epoxy as a crucial factor that impacts the performance of LED packages. However, it may have disregarded other significant factors like temperature, humidity, and mechanical loading conditions that could potentially influence the results in real-world applications. Finally, it is important to be cautious when applying the results of this study to other LED designs or encapsulant materials, as the findings may only apply to the specific LED package configuration and materials that were examined. Further investigation and validation are necessary to determine the generalizability of these findings. To advance the understanding and applicability of this study's findings in the field of LED packaging research and development, it is crucial to address these limitations and pursue the future directions identified.

4. Conclusions

The present study utilized the fluid-structure interaction (FSI) technique to examine the dynamics of interaction within an LED package, with specific emphasis on the correlation between the encapsulant and gold wire bonding. The numerical simulations were conducted to replicate the process of encapsulating LEDs and evaluate the influence of epoxy density on the performance of the package. The results indicated a positive correlation between epoxy density and the levels of gold wire deformation, von Mises stress, and elastic equivalent strain. In the encapsulant with the highest density (EMC), the maximum deformation of the gold wire, von Mises stress, and strain were measured as 2.6616×10^{-8} mm, 0.00064 MPa, and 8.2019×10^{-9} respectively. Remarkably, even with these levels of stress, the study discovered that the highest amount of stress on the gold wire bond did not reach a level that would significantly cause wire deformation or LED failure. These findings highlight the significance of epoxy density in the design of LED packages, indicating possible ways to improve LED reliability during operation by selecting the right materials and structural configurations. Subsequent investigations could delve into alternative materials or design strategies to reduce the negative effects of stress on the internal components of LED packages.

Acknowledgement

An acknowledgment to the Ministry of Higher Education Malaysia for the Fundamental Research Grant Scheme (FRGS) with the Project Code

of FRGS/1/2021/TK0/USM/03/9. The authors would also like to express their gratitude to Universiti Sains Malaysia for extending their assistance in a technical capacity.

REFERENCES

- [1] X. Long et al., A review on light-emitting diode based automotive headlamps. *Renewable and Sustainable Energy Reviews*. Elsevier Ltd, **41**, 29-41 (2015).
DOI: <https://doi.org/10.1016/j.rser.2014.08.028>
- [2] M. H. Chang, D. Das, P. V. Varde, M. Pecht, Light emitting diodes reliability review. *Microelectronics Reliability* **52**, 5, 762-782 (2012). DOI: <https://doi.org/10.1016/j.microrel.2011.07.063>
- [3] A. Nardelli, E. Deuschle, L.D. de Azevedo, J.L.N. Pessoa, E. Ghisi, Assessment of Light Emitting Diodes technology for general lighting: A critical review. *Renewable and Sustainable Energy Reviews* **75**, 368-379 Aug. (2017).
DOI: <https://doi.org/10.1016/j.rser.2016.11.002>
- [4] M.A. Alim, M.Z. Abdullah, M.S.A. Aziz, R. Kamarudin, Die attachment, wire bonding, and encapsulation process in LED packaging: A review. *Sensors and Actuators, A: Physical* **329**, (2021). DOI: <https://doi.org/10.1016/j.sna.2021.112817>
- [5] H. Xu, Y. Tang, J. Wu, B. Peng, Z. Chen, Z. Liu, The Study on Cracking Reasons of LED Encapsulation Silicone. in 2019 20th International Conference on Electronic Packaging Technology, ICEPT 2019, (2019).
DOI: <https://doi.org/doi:10.1109/icept47577.2019.245288>
- [6] X. Shan, Y. Chen, Experimental and modeling study on viscosity of encapsulant for electronic packaging. *Microelectronics Reliability* **80** (2018).
DOI: <https://doi.org/10.1016/j.microrel.2017.11.011>
- [7] M. Sadeghinia, K.M. Jansen, L.J. Ernst, Characterization of the viscoelastic properties of an epoxy molding compound during cure. *Microelectronics Reliability* **52**, 8 (2012).
DOI: <https://doi.org/10.1016/j.microrel.2012.03.025>
- [8] S.S.S. Ali, S.T.S. Hian, B.C. Ang, The effects of wire geometry and wire layout on wire sweep performance using LQFP packages in transfer mold. *International Journal of Precision Engineering and Manufacturing* **15**, 9, 1793-1799 (2014).
DOI: <https://doi.org/10.1007/s12541-014-0531-6>
- [9] D. Ramdan, Z.M. Abdullah, M.A. Mujeebu, W.K. Loh, C.K. Ooi, R.C. Ooi, FSI simulation of wire sweep PBGA encapsulation process considering rheology effect. *IEEE Trans Compon Packaging Manuf Technol* **2**, 4 (2012).
DOI: <https://doi.org/10.1109/tcpmt.2011.2171513>
- [10] H. Roslan et al., Analysis of LED wire bonding during encapsulation process. In *IOP Conference Series: Materials Science and Engineering*, (2020).
DOI: <https://doi.org/10.1088/1757-899X/1007/1/012173>
- [11] C.Y. Khor, M.Z. Abdullah, H.J. Tony Tan, W.C. Leong, D. Ramdan, Investigation of the fluid/structure interaction phenomenon in IC packaging. In *Microelectronics Reliability*, 241-252 (2012).
DOI: <https://doi.org/10.1016/j.microrel.2011.09.013>
- [12] C.Y. Khor, M.Z. Abdullah, Optimization of IC encapsulation considering fluid/structure interaction using response surface methodology. *Simul. Model Pract. Theory* **29**, 109-122 (2012).
DOI: <https://doi.org/10.1016/j.simpat.2012.07.003>
- [13] A. Husin, M.Z. Abdullah, A. Ismail, A.A. Janvekar, M.S. Rusdi, W.M.A.W.M. Ali, Heat transfer performance of a synthetic jet generated by diffuser-shaped orifice. *Journal of Advanced Research in Fluid Mechanics and Thermal Sciences* **53**, 1 (2019).
- [14] M.S. Rusdi et al., Numerical Investigation on the Effect of Squeegee Angle during Stencil Printing Process. *J. Phys. Conf. Ser.* **1082**, 1, 1-6 (2018).
DOI: <https://doi.org/10.1088/1742-6596/1082/1/012057>
- [15] C.Y. Khor, M.Z. Abdullah, H.J. Tony Tan, W.C. Leong, D. Ramdan, Investigation of the fluid/structure interaction phenomenon in IC packaging. *Microelectronics Reliability* **52**, 1, 241-252 (2012).
DOI: <https://doi.org/10.1016/j.microrel.2011.09.013>
- [16] E.E.S. Ong, M.Z. Abdullah, C.Y. Khor, W.K. Loh, C.K. Ooi, R. Chan, Analysis of encapsulation process in 3D stacked chips with different microbump array. *International Communications in Heat and Mass Transfer* **39**, 10, 1616-1623 (2012).
DOI: <https://doi.org/10.1016/j.icheatmasstransfer.2012.10.007>
- [17] W. Aniszewski, T. Ménard, M. Marek, Volume of Fluid (VOF) type advection methods in two-phase flow: A comparative study. *Comput Fluids* **97**, 52-73, Jun. (2014).
DOI: <https://doi.org/10.1016/j.compfluid.2014.03.027>
- [18] K. Choudhary et al., The joint automated repository for various integrated simulations (JARVIS) for data-driven materials design. *NPJ Comput Mater* **6**, 1, Dec. (2020).
DOI: <https://doi.org/10.1038/s41524-020-00440-1>
- [19] I. Chirica, C.M. Angheluta, S.D. Perijoc, A.I. Hobjilă, M. Frătita, Mesh independence of a transient multiphase fluid-solid interaction. In *Journal of Physics: Conference Series*, (2019).
DOI: <https://doi.org/10.1088/1742-6596/1297/1/012026>
- [20] J.C. Huang, Y.P. Chu, M. Wei, R.D. Deanin, Comparison of epoxy resins for applications in light-emitting diodes. *Advances in Polymer Technology* **23**, 4 (2004).
DOI: <https://doi.org/10.1002/adv.20018>
- [21] J.C. Huang, Y.P. Chu, M. Wei, R.D. Deanin, Comparison of epoxy resins for applications in light-emitting diodes. *Advances in Polymer Technology* **23**, 4, 298-306, Dec. (2004).
DOI: <https://doi.org/10.1002/adv.20018>
- [22] D.D. Lu, C.P. Wong, *Materials for advanced packaging*. (2009).
DOI: <https://doi.org/10.1007/978-0-387-78219-5>
- [23] Z. Chen, Y. Liu, S. Liu, Modeling of copper wire bonding process on high power LEDs. *Microelectronics Reliability* **51**, 1, 171-178 (2011). DOI: <https://doi.org/10.1016/j.microrel.2010.03.001>